H–He Demixing Driven by Anisotropic Hydrogen Diffusion

Xiaoju Chang[1,2], Dongdong Kang[1,2,3], Bo Chen[1,2,3*], and Jiayu Dai[1,2,3*]

[1]*College of Science, National University of Defense Technology, Changsha 410073, China*
[2]*Hunan Key Laboratory of Extreme Matter and Applications, National University of Defense Technology, Changsha 410073, China*
[3]*Hunan Research Center of the Basic Discipline for Physical States, National University of Defense Technology, Changsha 410073, China*

(Received 14 March 2025; accepted manuscript online 10 April 2025)

The dynamics of phase separation in H–He binary systems within gas giants such as Jupiter and Saturn exhibit remarkable complexity, yet lack systematic investigation. Through large-scale machine-learning-accelerated molecular dynamics simulations spanning broad temperature-pressure-composition (2000–10000 K, 1–7 Mbar, pure H to pure He) regimes, we systematically determine self and mutual diffusion coefficients in H–He systems and establish a six-dimensional framework correlating temperature, pressure, helium abundance, phase separation degree, diffusion coefficients, and anisotropy. Key findings reveal that hydrogen exhibits active directional migration with pronounced diffusion anisotropy, whereas helium passively aggregates in response. While the conventional mixing rule underestimates mutual diffusion coefficients by neglecting velocity cross-correlations, the assumption of an ideal thermodynamic factor ($Q = 1$) overestimates them due to unaccounted non-ideal thermodynamic effects—both particularly pronounced in strongly phase-separated regimes. Notably, hydrogen's dual role, anisotropic diffusion and bond stabilization via helium doping, modulates demixing kinetics. Large-scale simulations (216,000 atoms) propose novel phase-separation paradigms, such as "hydrogen bubble/wisp" formation, challenging the classical "helium rain" scenario, striving to bridge atomic-scale dynamics to planetary-scale phase evolution.

DOI: 10.1088/0256-307X/42/5/053704 CSTR: 32039.14.0256-307X.42.5.053704

Introduction. Hydrogen and helium, the most abundant elements in the universe, form the bulk of gas giants.[1] Their distribution, mixing states, and transport properties shape planetary interiors and evolution. In the solar system, Jupiter and Saturn exhibit layered structures: a molecular hydrogen envelope, a H–He mixed layer with possible helium rain, a metallic hydrogen region enriched in helium, and a dense or diffuse heavy-element core.[2] Atmospheric measurements reveal helium depletion compared to protosolar levels,[3–5] suggesting ongoing inward migration of helium. This is attributed to the fact that, under extreme pressure and temperature conditions, helium becomes immiscible in metallic hydrogen, forming dense droplets that "rain" toward the planet's core, releasing gravitational potential energy. This process, known as helium rain,[6] is a key mechanism for material transport, heat flow, and magnetic field generation,[7–10] making a detailed understanding of H–He diffusion crucial for modeling planetary interiors.

Recent experiments using laser-driven shock compression have shown the signal of H–He immiscibility at planetary conditions.[11] At the same time, advances in first-principle methods, from density functional theory (DFT) refinements[12–16] to quantum Monte Carlo benchmarks,[17] improve the accuracy. Thermodynamic integration achieve non-ideal entropy calculations.[18] The large-scale ($\sim$ 10000 atoms) machine-learning-assisted simulations[19] provide structural diagnostics of phase separation, consistently supporting the presence of a H–He miscibility gap despite uncertainties in demixing temperatures.

While phase separation thermodynamics is widely studied, the microscopic dynamics, especially the coupling between phase separation and transport behaviors, remains unclear, which is a critical knowledge gap as diffusion coefficients characterize atomic mobility and directly reflect phase separation evolution. For pure hydrogen, path-integral molecular dynamics with DFT has shown abrupt changes in electrical conductivity[20] and self-diffusion coefficients at liquid–liquid phase transitions (LLPT), and has highlighted nuclear quantum effects.[21] In H–He mixtures, Soubiran *et al.*[22] found that trace heavy elements have negligible effects on hydrogen and helium self-diffusion. French *et al.*[23] compiled self-diffusion coefficients data along Jupiter's adiabatic path, revealing abrupt changes due to hydrogen dissociation and ionization but neglecting mutual diffusion and compositional gradients from phase separation. Li *et al.*[24] conducted the first systematic quantum molecular dynamics (QMD) study of self and mutual diffusion across extreme thermodynamic conditions, demonstrating that phase separation induces non-Fickian behavior and causes deviation of the

*Corresponding author. Email: chenbochain@nudt.edu.cn; jydai@nudt.edu.cn
© 2025 Chinese Physical Society and IOP Publishing Ltd. All rights, including for text and data mining, AI training, and similar technologies, are reserved.

Stokes-Einstein relation from its constant value. Nevertheless, the assumption of ideal mixing (thermodynamic factor $Q = 1$) for mutual diffusion calculations should be an approximation invalid in phase-separated systems. A subsequent QMD study [25] refined diffusion coefficients via more accurate double-exponential fitting but remained limited to a single density ($1.0\,\mathrm{g/cm^3}$), small system sizes (~ 200 atoms), and non-phase-separated conditions, leaving the key modulation mechanisms unexplored under the conditions of gas giants.

The present study focuses on the diffusion behaviors of H–He mixtures under phase separation using deep learning potentials (DLP),[26–28] where neural networks represent the potential energy surface as the sum of atomic energies determined by local chemical environments. This approach eliminates the iterative electronic structure calculations required in traditional first-principles molecular dynamics, reducing computational complexity scaling from cubic to linear order with system size. The methodology has been proved effective and efficient in investigating transport properties of materials under extreme conditions.[29–31] Enabled by deep potential molecular dynamics, we systematically conduct large-scale, long-time, and multi-replica simulations with first-principles accuracy to calculate self and mutual diffusion coefficients. By using phase separation data from Ref. [19], for the first time, we have mapped the relationship between phase separation extent and diffusion coefficients, and quantified diffusion anisotropy. Additionally, we compute the non-ideal thermodynamic factor and assess the applicability of the mixing-rule approach,[32] detecting a nonlinear modulation effect of phase separation gradients on mutual diffusion.[33] These findings not only refine computational methodologies but also provide fundamental insights into hydrogen and helium transport in giant planetary interiors.

Methods. The self-diffusion coefficient D_α can be calculated from the mean square displacement (MSD),[34]

$$D_\alpha = \frac{\langle |\boldsymbol{r}_i(t) - \boldsymbol{r}_i(0)|^2 \rangle}{6t}. \tag{1}$$

Equivalently, it can be obtained by integrating the velocity autocorrelation function (VACF) over time,[35]

$$D_\alpha = \frac{1}{3N_\alpha} \sum_{i=1}^{N_\alpha} \int_0^\infty \langle \boldsymbol{u}_i(t) \cdot \boldsymbol{u}_i(0) \rangle \, \mathrm{d}t, \tag{2}$$

where $\boldsymbol{r}_i(t)$ and $\boldsymbol{u}_i(t)$ are the coordinate and velocity vectors of the i-th particle of element α at time t, and N_α is the number of particles of component α. The significant statistical fluctuations inherent in single VACF calculations often lead to unstable convergence, rendering it unsuitable for direct quantitative analysis of anisotropic characteristics. Thus, here we employ the MSD method for analyzing self-diffusion coefficients. The coefficient of variation (CV) is used to quantify anisotropic, which is mathematically defined as

$$CV_\alpha = \left\langle \frac{\sqrt{\frac{1}{3}\sum_{i\in\{x,y,z\}} (D_\alpha^i - \overline{D_\alpha})^2}}{\overline{D_\alpha}} \right\rangle_{\mathrm{MD}}, \tag{3}$$

where $\overline{D_\alpha} = \frac{1}{3}\sum_{i\in\{x,y,z\}} D_\alpha^i$ is the average of the self-diffusion coefficients in the three directions. The angle brackets denote the average over multiple independent MD simulations. The larger the CV, the stronger the anisotropy of diffusion.

In a binary system, the mutual diffusion coefficient $D_{\alpha\beta}$ between elements α and β is expressed as[32]

$$D_{\alpha\beta} = \frac{Q}{3N x_\alpha x_\beta} \int_0^\infty \langle \boldsymbol{j}^r(t) \cdot \boldsymbol{j}^r(0) \rangle \, \mathrm{d}t, \tag{4}$$

where x_α and x_β are the molar fractions of the two elements, N is the total number of atoms in the system, and $\boldsymbol{j}^r$ represents the relative particle flux,

$$\boldsymbol{j}^r(t) = x_\beta \boldsymbol{j}^\alpha(t) - x_\alpha \boldsymbol{j}^\beta(t), \tag{5}$$

where $\boldsymbol{j}^\alpha(t) = \sum_{i=1}^{N_\alpha} \boldsymbol{u}_i(t)$. The parameter Q describes the thermodynamic behavior of the mixture,

$$Q = \frac{1}{1 + x_\alpha x_\beta \rho (\Gamma_{\alpha\alpha} + \Gamma_{\beta\beta} - 2\Gamma_{\alpha\beta})}, \tag{6}$$

where ρ is the total particle number density, and $\Gamma_{\alpha\beta}$ is the integral of the radial distribution function $g_{\alpha\beta}(r)$,

$$\Gamma_{\alpha\beta} = 4\pi \int_0^\infty r^2 [g_{\alpha\beta}(r) - 1] \, \mathrm{d}r. \tag{7}$$

For thermodynamically ideal mixtures, the three radial distribution functions are identical ($\Gamma_{\alpha\alpha} = \Gamma_{\beta\beta} = \Gamma_{\alpha\beta}$), resulting in $Q = 1$. Notably, in systems undergoing phase separation, Q must be rigorously calculated to ensure accuracy.

$D_{\alpha\beta}$ can also be estimated using self-diffusion coefficients and the mixing-rule. By categorizing velocity autocorrelation and cross-correlation terms, Eq. (4) can be rewritten as

$$\begin{aligned} D_{\alpha\beta} = Q\Big[& x_\beta D_\alpha + x_\alpha D_\beta \\ & + x_\alpha x_\beta \Big(\frac{f_{\alpha\alpha}}{x_\alpha^2} + \frac{f_{\beta\beta}}{x_\beta^2} - 2\frac{f_{\alpha\beta}}{x_\alpha x_\beta} \Big) \Big], \end{aligned} \tag{8}$$

where the cross-correlation term is defined as

$$f_{\alpha\beta} = \frac{1}{3N} \sum_{i=1}^{N_\alpha} \sum_{j\neq i}^{N_\beta} \int_0^\infty \langle \boldsymbol{u}_i(t) \cdot \boldsymbol{u}_j(0) \rangle \, \mathrm{d}t. \tag{9}$$

Assuming velocity cross-correlations vanish,

$$\frac{f_{\alpha\alpha}}{x_\alpha^2} + \frac{f_{\beta\beta}}{x_\beta^2} - 2\frac{f_{\alpha\beta}}{x_\alpha x_\beta} = 0, \tag{10}$$

which yields the simplified Darken equation,[36]

$$D_{\alpha\beta} = Q(x_\beta D_\alpha + x_\alpha D_\beta). \tag{11}$$

The applicability of mixing-rule method on present systems is further examined in the subsequent sections of this work.

In this study, we employed the DLP from Ref. [19], which is based on the SCAN+rVV10 functional.[37,38] This DLP covers temperatures from 1000 K to 13000 K, pressures from 0.5 Mbar to 10 Mbar, and helium abundances

(x_{He}) from 0 to 1. The MD simulations were designed to capture the multiscale behavior of H–He mixtures under planetary conditions. We use 960-atom systems, with x_{He} being 0, 0.375, 0.5, 0.625, and 1, at pressures of 1, 2, 4, and 7 Mbar, and temperatures from 2000 K to 10000 K in 2000 K steps, respectively. For each condition, 20 independent simulations (30000 steps, 0.2 fs time step) with different initial random number seeds were conducted using LAMMPS,[39] with 1 ps for equilibration and 5 ps for data collection. The integration cutoff time for mutual diffusion coefficient is 2 ps, and the double-exponential model is used to enhance accuracy. Tests of size, trajectory length, and simulation repetitions are in Supplementary Materials.[40]

Results. Figure 1 presents the self-diffusion coefficients of hydrogen (D_{H}) and helium (D_{He}) across the full parameter space, plotted as functions of pressure. Given that D_{H} is an order of magnitude higher than D_{He}, they are displayed separately. The degree of phase separation $\Delta x = x_{\mathrm{He-rich}} - x_{\mathrm{He-poor}}$ represents the abundance difference for helium in He-rich and He-poor zones.[19] According to the figure, self-diffusion coefficients increase with temperature and decrease with pressure. This is consistent with classical diffusion theory, which attributes thermal activation to increased atomic mobility and densification to suppressed motion through enhanced intermolecular interactions. Notably, x_{He} introduces non-trivial dependencies in diffusion coefficients. For instance, at 6000 K and 4 Mbar [Figs. 1(c1)–1(c4)], D_{H} drops significantly from $x_{\mathrm{He}} = 0$ [Fig. 1(c1)] to $x_{\mathrm{He}} = 0.375$ [Fig. 1(c2)], then declines more gradually at higher x_{He}. This trend is corroborated by radial distribution functions (RDFs) in Fig. 2(a1), where hydrogen's first RDF peak shifts leftward and sharpens with increasing x_{He}. The synchronized rates between D_{H} reduction and RDFs' peak shift suggest an enhanced "hydrogen bonding effects" introduced by helium.

At 2000 K, hydrogen self-diffusion coefficients exhibit fundamentally different pressure-dependent behavior than that in high-temperature regimes, manifesting distinct non-monotonic characteristics, as illustrated in Figs. 1(e1)–1(e4). In pure hydrogen [Fig. 1(e1)], D_{H} displays pressure-induced anomalies with initial increases followed by decreases. This abnormal behavior originates from the LLPT: molecular dissociation occurring at 1–2 Mbar enhances atomic mobility, but at higher pressures, densification suppresses motion. Remarkably, the presence of helium induces a pressure-threshold shift in hydrogen dissociation through strengthening hydrogen bonding. At $x_{\mathrm{He}} = 0.375$ [Fig. 2(b1)], molecular hydrogen persists at 2 Mbar, delaying dissociation and enabling continuous D_{H} increase across 2–4 Mbar [Fig. 1(e2)]. When it comes to $x_{\mathrm{He}} = 0.5$, a very weak molecular signature peak emerges at 4 Mbar [Fig. 2(b2)], creating a local D_{H} maximum [Fig. 1(e3)]. At $x_{\mathrm{He}} = 0.625$ [Fig. 2(b3)], this threshold delayes to 7 Mbar, further modifying D_{H} trends [Fig. 1(e4)]. This pressure-composition competition highlights how helium stabilizes hydrogen bonding and alters hydrogen diffusion behavior. This mechanism may explain the reduced phase separation with increasing x_{He}, as molecular hydrogen stabilization weakens the thermodynamic driving force for demixing, consistent with Ref. [19].

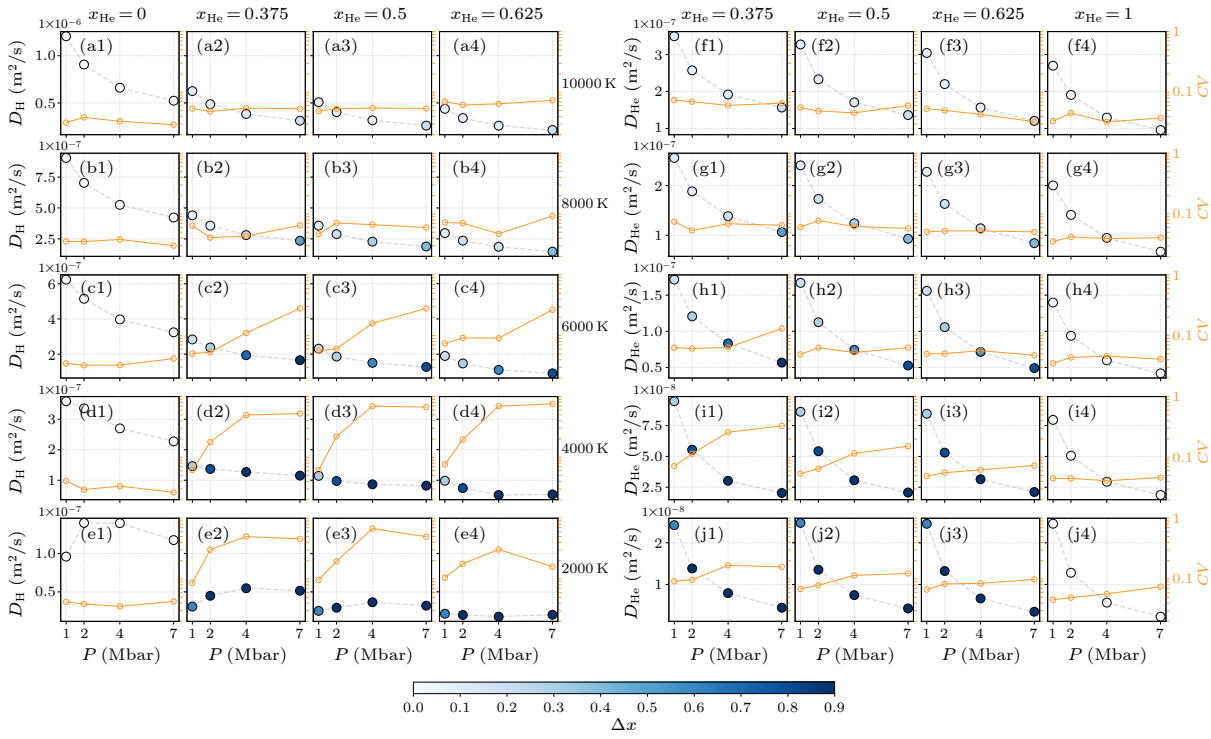

Fig. 1. Self-diffusion coefficients. The left panel shows D_{H} and the right panel shows D_{He}. The color maps the degree of phase separation Δx, with darker shades of blue indicating stronger separation. Subfigures sharing the same alphabetic prefix use a common left axis for comparability under isothermal conditions, and all subplots share the right vertical axis representing CV.

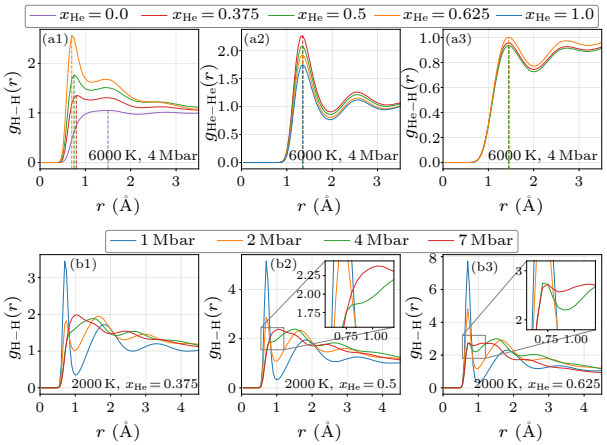

Fig. 2. Radial distribution function (RDF). (a1), (a2), and (a3): RDFs of H–H, He–He, and He–H at 6000 K, 4 Mbar, with varying helium abundance, respectively. Vertical dashed lines in these figures are the first-peak positions. (b1), (b2), and (b3): H–H RDFs at 2000 K with varying pressure.

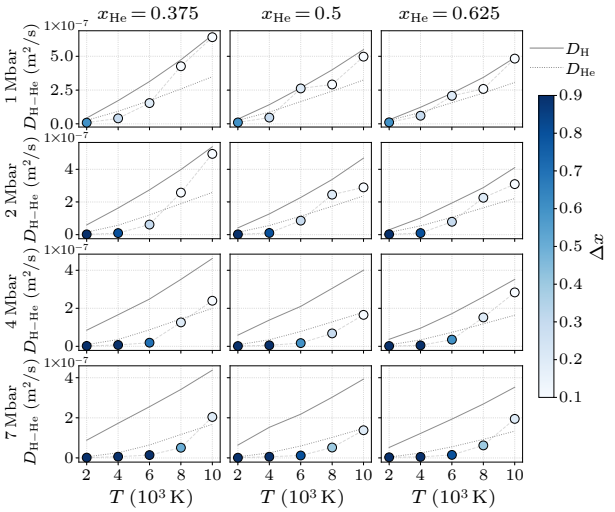

Fig. 3. Mutual diffusion coefficients. The color maps Δx. D_H and D_{He} are plotted as gray solid and dotted lines. Subplots with the same pressure share the same left axis.

Compared with hydrogen, D_{He} also decreases as x_{He} increases, but to a lesser extent. Helium RDFs [Fig. 2(a2)] and H–He cross-RDFs [Fig. 2(a3)] show stable peak positions, indicating no significant structural reorganization. A closer look at Fig. 1 reveals a correlation between phase separation and helium diffusion suppression: in weakly phase-separated regions (light-colored, low-pressure/high-temperature), D_{He} declines sharply with x_{He}, whereas in strongly phase-separated regimes (dark-colored, high-pressure/low-temperature), this effect weakens. More direct comparisons of this phenomenon are presented in Supplementary Materials.[40] This suggests a "H–He drag effect", where hydrogen transfers kinetic energy to helium. As x_{He} increases, reduced hydrogen limits the total transferred energy, which is simultaneously diluted among more helium atoms. Phase separation further modulates this process: in homogeneous mixtures, sufficient H–He contact enhances momentum dissipation, leading to synchronized diffusion reductions. In phase-separated regions, reduced H–He contact confines energy transfer to interfaces, mitigating helium diffusion suppression. Overall, D_H reduction is driven by helium-induced bonding effects, with supplementary drag effects from H–He interactions, whereas whereas D_{He} is mainly controlled by phase-separation-modulated kinetic energy transfer.

Regarding anisotropy, when significant phase separation occurs, it is typically associated with lower self-diffusion coefficients and higher anisotropy. Reduced diffusion enhances spatial localization, while increased anisotropy indicates directional rather than random motion, collectively facilitating phase separation. Remarkably, in significant phase-separated systems, hydrogen exhibits notably higher anisotropy than helium, suggesting that hydrogen diffusion predominantly drives phase separation, while helium aggregates more passively in response. Furthermore, as shown in Fig. 1, binary systems exhibit consistently higher CV values than their pure-element counterparts, and this effect is particularly pronounced in D_H. Such a phenomenon further supports the notion that in weakly phase-separated regions, hydrogen's active motion and high anisotropy serve as key drivers of early-stage phase separation.

For binary systems undergoing phase separation, the mutual diffusion coefficient (D_{H-He}) is a key parameter characterizing demixing kinetics. Figure 3 presents its temperature dependence. D_H and D_{He} are also plotted for comparisons. D_{H-He} generally increases with temperature and decreases with pressure, a trend consistent with D_H and D_{He}. However, their temperature-dependent growth rate exhibits a strong negative correlation with phase separation. When separation is pronounced, D_{H-He} deviates from the expected trend, plateauing below D_{He}. This indicates that mutual diffusion is significantly hindered, with hydrogen and helium preferentially diffusing within their respective enriched regions rather than permeating each other. As pressure decreases, phase separation weakens, and mutual diffusion is gradually restored.

Previous studies[24,25] assume the thermodynamic factor $Q = 1$. While reasonable for Ref. [25], which excludes phase separation, this assumption is invalid in Ref. [24], where mutual diffusion within phase-separated regions is explicitly examined. Reference [41] shows that in lamellar phases, self-RDF remains greater than 1 up to half of the lattice, as shown in Fig. 2(a1), whereas cross-RDF is below 1 as shown in Fig. 2(a3). According to Eq. (6), this causes Q to be significantly smaller than 1.

Beyond Q, another key aspect to consider is the applicability of mixing-rule method. Despite neglecting velocity correlations as in Eq. (10), this approach remains valuable due to its simplicity and efficiency.[42] It has shown good accuracy (error $< 15\%$) in weakly interacting systems such as liquid metals,[43–45] warm dense mixtures,[46] and plasmas.[47] The simple mixing model is particularly favored for multicomponent systems[48,49] due to its computational convenience. However, it should be noted that the applicability of mixing-rule is limited and requires thor-

ough validation. Local point defect equilibrium violates its major assumptions,[50] and high enthalpies of mixing exceed its descriptive capacity.[51] Moreover, asymmetric mixtures exhibit complex velocity cross-correlations, either positive[52] or negative,[53] introducing uncertainty in its accuracy.

To deconstruct the essential impact of computational model differences on non-ideal transport in H–He. Figure 4 compares $D_{\mathrm{H-He}}$ at $x_{\mathrm{He}} = 0.5$ and 7 Mbar using the full-simulation full-simulation versus mixing-rule methods. D_{H} and D_{He} are also plotted for comparisons. The ideal liquid mixing assumption $Q = 1$ introduces relative scaling errors up to 30 times across different temperatures, with calculations from 2000 K to 6000 K showing deviations by two orders of magnitude from actual values. With corrected Q values, the mixing-rule method still exhibits deviations reaching 80% in regions with significant phase separation, maintaining errors above 40% across the entire temperature systematic underestimation stems from positive H-He velocity cross-correlations. According to Eq. (10), this indicates stronger co-diffusion tendencies between like particles compared to unlike particles,[54] a phenomenon prevalent in present warm dense H–He systems[25] and particularly pronounced in significant phase separation regions. These findings highlight that the strong non-ideality of H–He mixtures under extreme conditions and their complex inter-component interactions result in significantly nonlinear characteristics in mass transport processes.

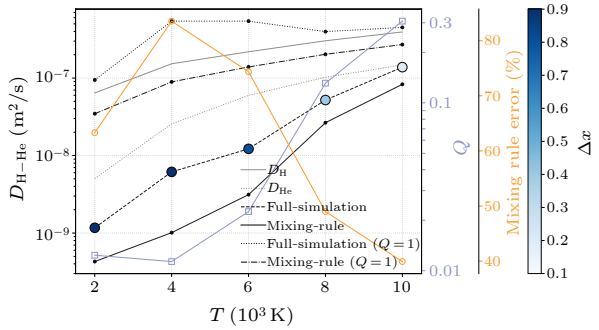

Fig. 4. Computational model differences. The first right vertical axis represents thermodynamic factor Q. The second right vertical axis represents mixing-rule error over full-simulation. The color maps Δx. D_{H} and D_{He} are plotted as gray solid and dotted lines.

Following systematic diffusion analysis, we investigated H–He phase separation in super large systems (216,000 atoms) after 40 ps relaxation. Figure 5(a) shows phase separation in equimolar H–He mixtures at 10 Mbar/3000 K, where hydrogen atoms form high-sphericity clusters. This aligns with Fig. 1's observation of stronger diffusion anisotropy in hydrogen versus helium, indicating that hydrogen actively coalesces into dense clusters while helium passively fills inter-cluster voids. This phase separation pattern diverges from the conventional "helium rain" sedimentation paradigm while better matching the dynamic picture of "hydrogen bubbles rise". At Jupiter and Saturn's helium abundance with a large demixing degree [Fig. 5(b): 2 Mbar/3000 K], phase separation remains hydrogen-dominated but forms irregular helium clusters with reduced sphericity compared to Fig. 5(a), reverting to classical "helium rain" behavior. As the temperature rises [Figs. 5(c) and 5(d): 2 Mbar/5000 and 6000 K], the weakened phase separation means hydrogen struggles to shape helium into well-defined clusters, the latter merely demonstrating differences in spatial distribution. In this case, it is hydrogen atoms who may form a flow network by stronger diffusional anisotropy, and the phase separation mode may evolve into a "hydrogen wisps rise" mechanism. Thus, the traditional "helium rain" model represents only a specific scenario with low helium abundance and significant phase separation. The entire evolutionary process of phase separation, or different regions within planetary interiors, exhibits multiple separation modes depending on helium abundance, temperature, and pressure. Mechanistically, the critical point lies in hydrogen's diffusion anisotropy, which always controls the demixing pathway. "Helium rain" requires passive helium aggregation under H-dominated dynamics, whereas "hydrogen bubble/wisp" mechanisms stem from active hydrogen self-organization.

It can be inferred from Figs. 5(c) and 5(d) that in the interiors of both Jupiter and Saturn, phase separation is mainly characterized by the slow upwelling of "hydrogen wisps", with helium serving as the background matrix. The degree of phase separation and the area where it occurs are significantly larger in Saturn than in Jupiter. From the perspective of planetary evolution, the change of helium abundance gradient caused by the upwelling of "hydrogen wisps" is more likely to lead to a greater degree of phase separation.

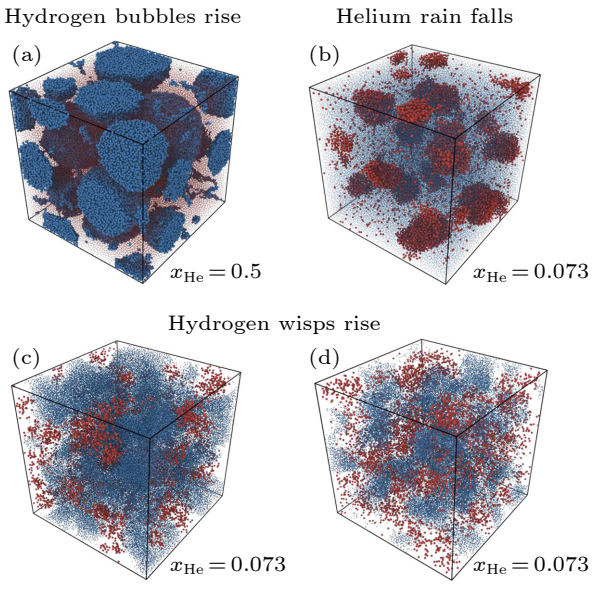

Fig. 5. Configurations of 216,000-atom systems and corresponding demixing mechanisms (blue: H; red: He). (a) $x_{\mathrm{He}} = 0.5$ (He radius reduced). (b) $x_{\mathrm{He}} = 0.073$ with significant phase separation (H radius reduced). (c) and (d) $x_{\mathrm{He}} = 0.073$ with weak phase separation, representing points near the adiabats of Saturn and Jupiter respectively (with the hydrogen radius reduced). The atomic screening method in Ref. [19] is employed to highlight the localized enrichment features.

Whether separation mechanisms such as "helium rain" or "hydrogen bubble" are triggered during evolution requires more comprehensive data support and refined modeling. These mechanistic interpretations, while consistent with diffusion data and structural configurations, remain speculative based on current evidence. Further experimental validation and larger-scale simulations are needed to confirm these mechanisms.

Conclusion. By establishing a six-dimensional mapping framework (T–P–x_{He}–Δx–D_α–CV_α), we elucidate the micro-kinetic mechanisms governing H–He phase separation. The D_{H} primarily responds to helium concentration-induced bond strengthening, coupled with Δx-controlled H–He mutual drag effects; the latter also affects D_{He}. This mechanistic insight may explain the observed suppression of phase separation with increasing helium concentration,[19] where elevated hydrogen molecular fractions counteract the driving forces of phase separation. Anisotropy analysis reveals hydrogen's dominant role in phase separation dynamics, exhibiting active directional migration versus helium's passive spatial aggregation. Hydrogen's hypermobility and pronounced anisotropy emerge as key drivers of incipient phase separation.

Additionally, by recalibrating the thermodynamic factor Q, we systematically determine mutual diffusion coefficients, revealing a plateau effect within phase separation regions. Comparative analysis with mixing-rule methodology demonstrates its inadequacy for current systems, where positive H–He velocity cross-correlation terms suggest stronger co-diffusion tendencies between like particles compared to unlike particles.

Ultimately, integrating equilibrium configurations of 216,000-atom systems with anisotropy characteristics, we propose novel phenomenological paradigms for H–He segregation across varying helium abundances and phase separation intensities.

Acknowledgements. This work was supported by the National University of Defense Technology Research Fund Project, the National Natural Science Foundation of China under Grant Nos. 12047561 and 12104507, the NSAF under Grant No. U1830206, the Science and Technology Innovation Program of Hunan Province under Grant No. 2021RC4026.

References

[1] Lodders K 2003 *ApJ* **591** 1220
[2] Helled R 2018 arXiv:1812.07436 [astro-ph.EP]
[3] von Zahn U, Hunten D M, and Lehmacher G 1998 *J. Geophys. Res. Planets* **103** 22815
[4] Mankovich C R and Fortney J J 2020 *ApJ* **889** 51
[5] Fortney J J 2004 *Science* **305** 1414
[6] Howard S, Müller S, and Helled R 2024 *Astron. Astrophys.* **689** A15
[7] Spohn T and Kaltenegger L 2015 *Heat Transfer, Planetary* (Berlin, Heidelberg: Springer Berlin Heidelberg) p. 1085
[8] Markham S and Guillot T 2024 *Planet. sci. j* **5** 269
[9] Qiu R, Zeng Q, Wang H, Kang D, Yu X, and Dai J 2023 *Chin. Phys. Lett.* **40** 116301
[10] Yang F, Zeng Q, Chen B, Kang D, Zhang S, Wu J, Yu X, and Dai J 2022 *Chin. Phys. Lett.* **39** 116301
[11] Brygoo S, Loubeyre P, Millot M, Rygg J R, Celliers P M, Eggert J H, Jeanloz R, and Collins G W 2021 *Nature* **593** 517
[12] Schöttler M and Redmer R 2018 *Phys. Rev. Lett.* **120** 115703
[13] Morales M A, Schwegler E, Ceperley D, Pierleoni C, Hamel S, and Caspersen K 2009 *Proc. Natl. Acad. Sci. U. S. A.* **106** 1324
[14] Lorenzen W, Holst B, and Redmer R 2011 *Phys. Rev. B* **84** 235109
[15] Militzer B 2013 *Phys. Rev. B* **87** 014202
[16] Kang D, Hou Y, Zeng Q, and Dai J 2020 *Matter Radiat. Extremes* **5** 055401
[17] Clay R C, Holzmann M, Ceperley D M, and Morales M A 2016 *Phys. Rev. B* **93** 035121
[18] Morales M A, Hamel S, Caspersen K, and Schwegler E 2013 *Phys. Rev. B* **87** 174105
[19] Chang X, Chen B, Zeng Q, Wang H, Chen K, Tong Q, Yu X, Kang D, Zhang S, Guo F, Hou Y, Zhao Z, Yao Y, Ma Y, and Dai J 2024 *Nat. Commun.* **15** 8543
[20] Lu B, Kang D, Wang D, Gao T, and Dai J 2019 *Chin. Phys. Lett.* **36** 103102
[21] van de Bund S, Wiebe H, and Ackland G J 2021 *Phys. Rev. Lett.* **126** 225701
[22] Soubiran F, Militzer B, Driver K P, and Zhang S 2017 *Phys. Plasmas* **24** 041401
[23] French M, Becker A C, Lorenzen W, Nettelmann N, Bethkenhagen M, Wicht J, and Redmer R 2012 *Astrophys. J. Suppl. Ser.* **202** 5
[24] Li D, Wang C, Kang W, Yan J, and Zhang P 2015 *Phys. Rev. E* **92** 043108
[25] Li Z G, Zhang W, Fu Z J, Dai J Y, Chen Q F, and Chen X R 2017 *Phys. Plasmas* **24** 052903
[26] Wang H, Zhang L, Han J, and E W 2018 *Comput. Phys. Commun.* **228** 178
[27] Zeng J, Zhang D, Lu D, Mo P, Li Z, Chen Y, Rynik M, Huang L, Li Z, Shi S, Wang Y, Ye H, Tuo P, Yang J, Ye D, Li Y, Tisi D, Zeng Q, Han B, Lei Y, Huang J, Muraoka K, Wang Y, Chang J, Yuan F, Bore S L, Cai C, Lin Y C, Wang B, Xu J, Zhu J, Luo C, Zhang Y, Rhys, Liang W, Singh A K, Yao S, Zhang J, Wentzcovitch R M, Han J, Liu J, Jia W, York D M, Weinan E, Car R, Zhang L, and Wang H 2023 *J. Chem. Phys.* **159** 054801
[28] Liu Q, Li J, and Chen M 2021 *Matter Radiat. Extremes* **6** 026902
[29] Sun H, Kang D, Hou Y, and Dai J 2017 *Matter Radiat. Extremes* **2** 287
[30] Qiu R, Zeng Q, Han J, Chen K, Kang D, Yu X, and Dai J 2025 *Phys. Rev. B* **111** 064103
[31] Zeng Q, Yu X, Yao Y, Gao T, Chen B, Zhang S, Kang D, Wang H, and Dai J 2021 *Phys. Rev. Res.* **3** 033116
[32] Zhou Y and Miller G H 1996 *J. Phys. Chem.* **100** 5516
[33] Zhang Y, Otani A, and Maginn E J 2015 *J. Chem. Theory Comput.* **11** 3537
[34] Einstein A 1905 *Ann. Phys. (Berlin, Ger.)* **17** 549
[35] Hansen J P and McDonald I R 2013 Chapter 9 - theories of time correlation functions *Theory of Simple Liquids* ed Hansen J P and McDonald I R (Oxford: Academic Press) p. 363
[36] Darken L S 1948 *Trans. Am. Inst. Min., Metall. Pet. Eng.* **175** 184
[37] Sun J, Ruzsinszky A, and Perdew J 2015 *Phys. Rev. Lett.* **115** 036402
[38] Sabatini R, Gorni T, and de Gironcoli S 2013 *Phys. Rev. B* **87** 041108

[39] Thompson A P, Aktulga H M, Berger R, Bolintineanu D S, Brown W M, Crozier P S, in 't Veld P J, Kohlmeyer A, Moore S G, Nguyen T D, Shan R, Stevens M J, Tranchida J, Trott C, and Plimpton S J 2022 *Comput. Phys. Commun.* **271** 108171
[40] See Supplementary Information for size effect, parameter convergence analysis and the correlation between phase separation and self diffusion suppression.
[41] Zhang K 2016 arXiv:1606.03610 [cond-mat.soft]
[42] Sridhar S 2010 *Metall. Mater. Trans. A* **41** 543
[43] Horbach J, Das S K, Griesche A, Macht M P, Frohberg G, and Meyer A 2007 *Phys. Rev. B* **75** 174304
[44] Rudd R E, Cabot W H, Caspersen K J, Greenough J A, Richards D F, Streitz F H, and Miller P L 2012 *Phys. Rev. E* **85** 031202
[45] Suzuki K, Yamada N, Tanka A, and Suzuki S 2014 *Trans. Jpn. Soc. Aeronaut. Space Sci.* **12** Ph_19
[46] Hou Y, Dai J, Kang D, Ma W, and Yuan J 2015 *Phys. Plasmas* **22** 022711
[47] Daligault J 2012 *Phys. Rev. Lett.* **108** 225004
[48] Krishna R and van Baten J 2005 *Ind. Eng. Chem. Res.* **44** 6939
[49] Liu X, Vlugt T J H, and Bardow A 2011 *Ind. Eng. Chem. Res.* **50** 10350
[50] Yurek G J and Schmalzried H 1974 *Ber. Bunsenges. Phys. Chem.* **78** 1379
[51] Atzmon M 1990 *Phys. Rev. Lett.* **65** 2889
[52] Haxhimali T, Rudd R E, Cabot W H, and Graziani F R 2014 *Phys. Rev. E* **90** 023104
[53] White A J, Ticknor C, Meyer E R, Kress J D, and Collins L A 2019 *Phys. Rev. E* **100** 033213
[54] Trullàs J and Padró J A 1994 *Phys. Rev. E* **50** 1162